Construction and Building Materials 114 (2016) 839–850

Contents lists available at ScienceDirect

Construction and Building Materials

journal homepage: www.elsevier.com/locate/conbuildmat

A multiphase micromechanical model for hybrid fiber reinforced concrete considering the aggregate and ITZ effects

Qing Chen [a,b,c,d], Hehua Zhu [b,c], Zhiguo Yan [b,c,*], J. Woody Ju [e], Zhengwu Jiang [a], Yaqiong Wang [d]

[a] Key Laboratory of Advanced Civil Engineering Materials (Tongji University), Ministry of Education, 1239 Siping Road, Shanghai 200092, China
[b] State Key Laboratory for Disaster Reduction in Civil Engineering, Tongji University, 1239 Siping Road, Shanghai 200092, China
[c] Key Laboratory of Geotechnical and Underground Engineering of the Ministry of Education, Tongji University, 1239 Siping Road, Shanghai 200092, China
[d] Shaanxi Provincial Major Laboratory for Highway Bridge and Tunnel, Chang'an University, Xi'an, Shaanxi 710064, China
[e] Department of Civil and Environmental Engineering, University of California, Los Angeles, CA 90095, USA

HIGHLIGHTS

- The presented framework can predict the properties of HFRC with the aggregate and ITZ effects.
- The properties of concrete and FRC can be calculated by the proposed micromechanical models.
- Different fibers can be considered by the multi-level homogenization scheme step by step.
- The homogenization sequence for different fibers has little influence on the predicting results.

ARTICLE INFO

Article history:
Received 7 July 2015
Received in revised form 31 March 2016
Accepted 2 April 2016
Available online 9 April 2016

Keywords:
Hybrid fiber reinforced concrete
Multi-level homogenization
Aggregate
Interfacial transition zone
Effective properties
Multi-phase micromechanical model

ABSTRACT

Very few micromechanical models are available for hybrid fiber reinforced concrete (HFRC), although it has been widely applied in many structures. To quantitatively predict the effective properties of HFRC with the aggregate and interfacial transition zone (ITZ) effects, a multi-phase micromechanical framework is proposed based on the material's microstructures. In the proposed model, the multi-types of fibers, aggregate, cement paste and ITZ are comprehensively considered. The volume fraction of the ITZ is analytically calculated based on the aggregate grading. Multi-level homogenization schemes are presented to predict the effective properties of HFRC. By utilizing the generalized self-consistent approach, the equivalent matrix composed by the aggregate, cement and the ITZ between them are obtained with the first and second level homogenization procedures. Through adding different types of fibers step by step into the equivalent matrix, the properties of HFRC are reached with the modifications to the Halpin-Tsai model. To demonstrate the feasibility of the proposed micromechanical framework, the predictions herein are compared with the experimental data, the Voigt upper bound and the Reuss lower bound. Finally, the influences of aggregate, ITZ, multi-types of fibers on the properties of HFRC are discussed based on the proposed micromechanical model.

1. Introduction

Fiber reinforced concrete (FRC) has been widely applied in many structures, such as frames, slabs, and tunnels, because the fiber addition in concrete can reduce the emergence and propagation of cracks, improve the mechanical behaviors, enhance the material's ductility, the impact resistance and the durability from the literatures [1–23].

Owing to the well-established performance of FRC, major efforts have been dedicated during the last decade to the modeling of its behavior. Empirical formulations to evaluate the elastic properties of concrete have been suggested by [24–28]. These formulations are obtained by means of laboratory tests, which is the phenomenological way to formulate the behavior of FRC. An attractive alternative to handle this kind of problem is provided by the framework of micromechanics, which reduces the laboratory expenses, meanwhile discloses the enhancing mechanism of fibers from the micro-scale level [29–33]. Teng et al. proposed a dedicated empirical formula for calculating the elastic moduli of steel fiber reinforced concrete(SFRC) through adopting the

* Corresponding author at: State Key Laboratory for Disaster Reduction in Civil Engineering, Tongji University, 1239 Siping Road, Shanghai 200092, China.
E-mail address: yanzguo@tongji.edu.cn (Z. Yan).

http://dx.doi.org/10.1016/j.conbuildmat.2016.04.008
0950-0618/

equivalent inclusion method [30]. Dutra et al. [29] proposed a micromechanical model for FRC and the linear elastic behavior is examined by implementation of a Mori–Tanaka homogenization scheme. Gal and Kryvoruk [31] employed the finite element method to analyze the properties of FRC using a two-step homogenization approach, where the *interfacial transition zone* (ITZ) between the aggregate and mortar is considered by a micromechanical homogenization process. Guan et al. [32] presented a stochastic micromechanical model to characterize the elastic modulus and Poisson's ratio of FRC.

Recently two or more types of fibers are usually added into the concrete to improve the material's performance, which is named by Hybrid fiber reinforced concrete (HFRC) [33–40]. Unfortunately, the current micromechanical models for FRC only consider one kind of fiber [29–32], very few micromechanical models for HFRC can be reached according to the author's studies. Furthermore, presently little attention is paid to the quantitative influence of the aggregate and ITZ on the properties of FRC [31], not to mention on those of HFRC. To address these issues in this extension, a multiphase micromechanical framework based on the material's microstructure is proposed to analytically investigate the mechanical performance of HFRC considering the aggregate and ITZ effects. A new multi-level homogenization scheme is presented to consider the effects of multi-types of fibers. Meanwhile, quantitative influences of aggregate and ITZ on the properties of HFRC are taken into consideration with the proposed homogenization framework and analytical calculations for the ITZ volume fraction.

The rest of this paper is organized as follows. In Section 2, a multiphase micromechanical model for the HFRC is presented based on the material's microstructures. Section 3 introduces the micromechanical representations for the ITZ, including its properties and the analytical calculations for its volume fractions. In Section 4, multilevel homogenization procedures are proposed to estimate the effective properties of HFRC. Numerical examples including experimental validations and comparisons with existing models are presented in Section 5, which also discusses the influences of the aggregate, ITZ and fibers on the macroscopic properties of HFRC based on the proposed micromechanical framework in this study. And some conclusions are reached in the final section.

2. Multiphase micromechanical model for HFRC

2.1. Microstructure of HFRC

Concretes are heterogeneous in nature and generally consist of different constituents or phases, such as aggregate, cement paste and C-S-H [41–45]. Further, the constituents of materials can be treated as homogeneous at a certain length scale, but when observed at a smaller length scale, the constituents themselves may become heterogeneous, i.e. a multi-scale phenomenon for heterogeneous concrete. For examples, the concrete can be treated as the homogenous material at the macroscopic material. At the lower level, the coarse aggregates are embedded in the mortar matrix, which can be treated as two-phase composite composed of the cement pastes and the sand particles. Moreover, the cement pastes are formed by homogeneous C-S-H with large CH crystals, aluminates, cement clinker and water [41,42]. Due to these heterogeneous and multi-scale natures, it is usually impractical and often impossible to describe all the precise characters of the microstructure of concrete. To investigate the ITZ effects on the concrete properties, the concrete are usually described by three phase material consisting of the bulk cement phase, the aggregates (sand and rock) and the ITZ between them [43–45], which implies that the lower length scale structures, like C-S-H, CH crystals and aluminates, etc., are not taken into considerations.

To predict the properties of HFRC with the ITZ effects, the microstructures of the HFRC are characterized by embedding the hybrid fibers into the three phrase material proposed by [43–45], which means HFRC is described by a multiphase composite formed by the bulk cement paste, aggregates, different types of fibers and ITZs in the present study.

2.2. Micromechanical model for hybrid fiber reinforced concrete

According to the previous studies [42–45], to simply the analysis, the shape of the aggregate is presumed to be spherical, although the geometry of the aggregates is quite complex in reality. The fibers are randomly distributed within concrete. They can be represented by a set of flat prolate spheroids which differ in orientations [29]. The interfaces between fibers and the cement paste are presumed to be well bonded [29–31]. Actually, there are ITZs between the fibers and concrete, which may deteriorate the effective properties of HFRC [46,47]. In this paper, we follow the assumption that the interface between the fibers and concrete is perfect according to many previous researches [29–31]. The quantitative effects of these ITZs between the fibers and concrete will be carefully investigated in our coming works.

Using the aforementioned assumptions, a multiphase micromechanical model for HFRC is proposed, as displayed in Fig. 1. The inner sphere is the aggregate phase, surrounded by a concentric ITZ shell. The aggregate and the ITZ shells are embedded in bulk paste matrix, where the shell elements are homogeneous and isotropic in composition and mechanical property. The hybrid fibers are randomly distributed in the ITZ and bulk paste matrix. By predicting the effective properties of the proposed model, the HFRC's macroscopic mechanical performance is revealed theoretically and quantitatively from its microstructures. It is noted that the effects of the different fiber lengths are not taken into considerations for simplification purposes in this study since they very slightly affects the moduli of fiber reinforced concrete according to the previous studies [11,13,25,29,30].

3. Micromechanical representations for the ITZ

3.1. The properties of the ITZ

The restrained placement of cement around aggregates results in a gradient of porosity, and therefore a gradient of properties, around each aggregate [48]. It seems reasonable that the ITZ can be divided into multi-layered spherical shells whose composition and properties are allowed to vary with distance from the aggregate surface and with the progress of hydration [43–45,48]. However, it is hard to get the exact gradient of ITZ properties, and different assumptions for the ITZ properties distribution are utilized in the previous work [43–45]. For simplifications, the ITZ

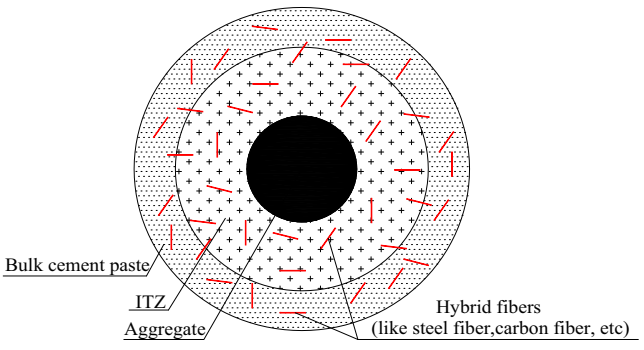

Fig. 1. Multi-phase micromechanical model for hybrid fiber reinforced concrete (HFRC).

in this paper is represented by a single shell of uniform property as shown in Fig. 1 based on [49]. Three parameters are utilized to character its properties, including one geometrical quantity to describe its thickness and two mechanical constants (the Young's modulus and Poisson's ratio).

3.2. The volume fraction of the ITZ

The high volume fraction of aggregates in a typical concrete (60–75%) means that the spacing between adjacent aggregates is only a few times the typical ITZ thickness [48]. The volume fraction of ITZ is then computed, taking into account the overlapping of ITZ shells, using the 'void exclusion probability' derived by [50] and applied to concrete systems by [43–45,48,51].

As to the proposed multiphase micromechanical model for HFRC, the void exclusion probability means the fraction of the bulk paste, which can be expressed as below [45,48]:

$$c_{bk} = (1 - c_{ag}) \exp(-\pi\rho(\alpha t + \beta t^2 + \gamma t^3)) \tag{1}$$

$$\alpha = \frac{4\overline{R^2}}{1 - c_{ag}} \tag{2}$$

$$\beta = \frac{4\bar{R}}{1 - c_{ag}} + \frac{12\varepsilon_2\overline{R^2}}{(1 - c_{ag})^2} \tag{3}$$

$$\gamma = \frac{4}{3(1 - c_{ag})} + \frac{8\varepsilon_2\bar{R}}{(1 - c_{ag})^2} \tag{4}$$

$$\varepsilon_2 = \frac{2\pi\rho\overline{R^2}}{3} \tag{5}$$

where c_{bk} and c_{ag} are the volume fractions for the bulk cement paste and aggregate (sand and rock), respectively; ρ is the total number of aggregate per unit volume, and α, β and γ are functions of the mean aggregate radius $\bar{R}$ and the mean square aggregate radius $\bar{R}^2$ according to the aggregate size distribution. According to [45,52], with the assumption of uniform distribution by volume of aggregates, the remaining parameters are calculated from aggregate size distribution as:

$$\rho = \sum_{i=1}^{M} \frac{9c_{ag}c_i}{4\pi(r_{i+1}^3 - r_i^3)} \ln\left(\frac{r_{i+1}}{r_i}\right) \tag{6}$$

$$\bar{R} = \sum_{i=1}^{M} \frac{9c_{ag}c_i}{4\pi\rho(r_{i+1}^3 - r_i^3)} (r_{i+1} - r_i) \tag{7}$$

$$\overline{R^2} = \sum_{i=1}^{M} \frac{9c_{ag}c_i}{4\pi\rho(r_{i+1}^3 - r_i^3)} \frac{1}{2} (r_{i+1}^2 - r_i^2) \tag{8}$$

where c_i is the volume fraction of aggregates with radius ranging from r_i to r_{i+1}. The volume fraction of the ITZ is finally obtained by simple subtraction:

$$c_{itz} = 1 - c_{ag} - c_{bk} - c_{hf} \tag{9}$$

where c_{hf} is the volume fraction of hybrid fibers. It is the sum for the volume fractions of different fibers.

4. Estimating the effective properties of HFRC

4.1. Multilevel homogenization scheme for estimating effective properties

Micromechanical models for estimating the effective properties of the composite are usually developed by averaging the stress field and strain field of the material representative volume element (RVE) featuring a "mesoscopic" length scale which is much larger than the characteristic length scale of particles (inhomogeneities) but smaller than the characteristic length scale of a macroscopic specimen. Mathematically, this procedure is related to the homogenization method [54]. Previously published studies have shown that a homogenization stepping scheme is an effective way to obtain the effective properties of multi-inclusion composites [49,53–73]. The multiphase micromechanical model used in the present study also employs a multilevel homogenization procedure. First, the three phase sphere model presented by Christensen and Lo [74] is employed to homogenize the two-phase composite composed of the aggregate and ITZ into the equivalent inclusions, as shown in Fig. 2(a). Second, the first equivalent matrix is obtained by homogenizing the two-phase composite composed of the bulk cement paste and the equivalent inclusion obtained in the first level homogenization with Christensen and Lo's model [74] again, as exhibited in Fig. 2(b). Due to the spherical symmetry, the equivalent material present after this homogenization is still isotropic. Third, by averaging the lower bounds and upper bounds of the Halpin-Tsai model [75], the effective properties of the second equivalent matrix can be obtained by the homogenization of the two-phase composite composed of the first equivalent matrix and the first kind fiber, as shown in Fig. 2(c). When the ith kind of fiber is considered, the $(i+1)$th equivalent matrix will be reached by the $(i+2)$th level homogenization with the ith equivalent matrix obtained by the $(i+1)$th level homogenization, as displayed in Fig. 2(d). If there are n kinds of fibers, the properties of the HFRC can be calculated by the $(n+2)$th level homogenization. Take the concrete reinforced by the steel and carbon fiber as an example ($n = 2$). After the first and second level homogenization, the first equivalent matrix has been reached. Let's consider the steel fiber firstly ($i = 1$). The *second* equivalent matrix (composed by the *first* equivalent matrix and steel fiber) will be reached by the *third* level homogenization with the *first* equivalent matrix obtained by the *second* level homogenization. For the carbon fiber ($i = 2 = n$), the properties of the HFRC can be calculated by *forth* level homogenization with the *second* equivalent matrix obtained by the *third* level homogenization.

4.2. The first-level homogenization for the equivalent inclusion composed of aggregate and ITZ

The first-level homogenization employs the three-phase sphere model to obtain the effective bulk modulus and shear modulus of the equivalent inclusion. For the two-phase composite made up of the aggregates (as the inner material) and ITZ (as the outer material), the effective properties can be reached based on Christensen and Lo's work [74], which can be expressed as below:

$$K_F = K_{itz} + \frac{\phi_{ag}(K_{ag} - K_{itz})(3K_{itz} + 4\mu_{itz})}{3K_{itz} + 4\mu_{itz} + 3(1 - \phi_{ag})(K_{ag} - K_{itz})} \tag{10}$$

$$A\left(\frac{\mu_F}{\mu_{itz}}\right)^2 + B\left(\frac{\mu_F}{\mu_{itz}}\right) + C = 0 \tag{11}$$

with

$$\begin{aligned} A = {} & 8\left(\frac{\mu_{ag}}{\mu_{itz}} - 1\right)(4 - 5v_{itz})\eta_1\phi_{ag}^{10/3} - 2\left[63\left(\frac{\mu_{ag}}{\mu_{itz}} - 1\right)\eta_2 + 2\eta_1\eta_3\right]\phi_{ag}^{7/3} \\ & + 252\left(\frac{\mu_{ag}}{\mu_{itz}} - 1\right)\eta_2\phi_{ag}^{5/3} - 50\left(\frac{\mu_{ag}}{\mu_{itz}} - 1\right) \\ & \times (7 - 12v_{itz} + 8v_{itz}^2)\eta_2\phi_{ag} + 4(7 - 10v_{itz})\eta_2\eta_3 \end{aligned} \tag{12}$$

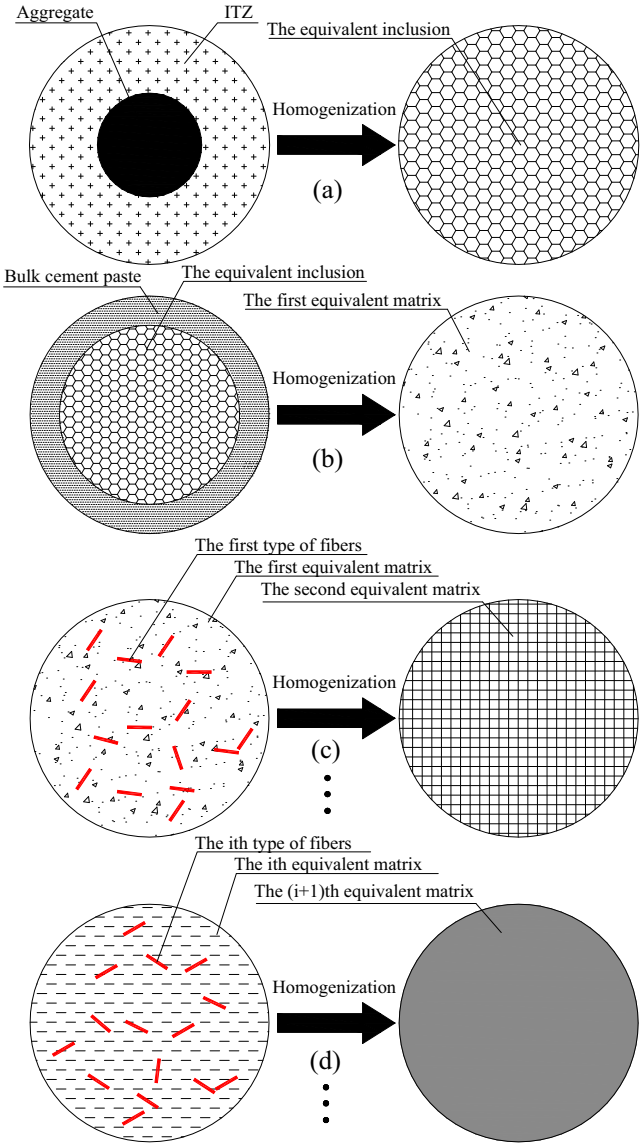

Fig. 2. The multilevel homogenization procedures: (a) the first-level: homogenization of the aggregate and ITZ; (b) the second-level: homogenization of the bulk cement paste and equivalent inclusion; (c) the third-level: homogenization of the first equivalent matrix and the first type of fibers; (d) the $(i+2)$-level: homogenization of the ith equivalent matrix and the ith type of fibers. Here $i = 1,2\ldots n$, with n being the sum of the fiber types. The equivalent HFRC can be reached by the $(n+2)$th-level homogenization.

$$B = -4\left(\frac{\mu_{ag}}{\mu_{itz}} - 1\right)(1 - 5v_{itz})\eta_1\phi_{ag}^{10/3} + 4\left[63\left(\frac{\mu_{ag}}{\mu_{itz}} - 1\right)\eta_2 + 2\eta_1\eta_3\right]\phi_{ag}^{7/3} - 504\left(\frac{\mu_{ag}}{\mu_{itz}} - 1\right)\eta_2\phi_{ag}^{5/3} + 150\left(\frac{\mu_{ag}}{\mu_{itz}} - 1\right)(3 - v_{itz})v_{itz}\eta_2\phi_{ag} + 3(15v_{itz} - 7)\eta_2\eta_3 \quad (13)$$

$$C = 4\left(\frac{\mu_{ag}}{\mu_{itz}} - 1\right)(5v_{itz} - 7)\eta_1\phi_{ag}^{10/3} - 2\left[63\left(\frac{\mu_{ag}}{\mu_{itz}} - 1\right)\eta_2 + 2\eta_1\eta_3\right]\phi_{ag}^{7/3} + 252\left(\frac{\mu_{ag}}{\mu_{itz}} - 1\right)\eta_2\phi_{ag}^{5/3} + 25\left(\frac{\mu_{ag}}{\mu_{itz}} - 1\right)(v_{itz}^2 - 7)\eta_2\phi_{ag} - 3(7 + 5v_{itz})\eta_2\eta_3 \quad (14)$$

$$\eta_1 = \left(\frac{\mu_{ag}}{\mu_{itz}} - 1\right)(49 - 50v_{ag}v_{itz}) + 35\left(\frac{\mu_{ag}}{\mu_{itz}}\right)(v_{ag} - 2v_{itz}) + 35(2v_{ag} - v_{itz}) \quad (15)$$

$$\eta_2 = 5v_{ag}\left(\frac{\mu_{ag}}{\mu_{itz}} - 8\right) + 7\left(\frac{\mu_{ag}}{\mu_{itz}} + 4\right) \quad (16)$$

$$\eta_3 = \frac{\mu_{ag}}{\mu_{itz}}(8 - 10v_{itz}) + (7 - 5v_{itz}) \quad (17)$$

$$\phi_{ag} = \frac{c_{ag}}{c_{ag} + c_{itz}} \quad (18)$$

where K_F and μ_F are the effective bulk modulus and shear modulus of the equivalent inclusions after the first level homogenization, ϕ_{ag} is the volume fraction of aggregates in the two-phase composite made up of the aggregate and ITZ, K_{ag}, μ_{ag} and v_{ag} (K_{itz}, μ_{itz} and v_{itz}) are the bulk modulus, shear modulus and Poisson's ratio for the aggregates (the ITZ).

4.3. The second-level homogenization for the concrete composed of the cement paste and equivalent inclusion

As to the concrete consisting of the cement paste and the equivalent inclusion, the material's effective mechanical properties can be similarly obtained by employing the three-phase sphere model [74]. Let K_{bk}, μ_{bk} and v_{bk} signify the bulk modulus, shear modulus and Poisson's ratio of the bulk cement paste and v_F be the effective Poisson's ratio of the equivalent inclusions. The effective properties of the three phase composite, including the aggregates, the ITZ and the bulk cement paste, can be reached by following alterations to Eqs. (10)–(18): Firstly, K_{itz}, μ_{itz} and v_{itz} (K_{ag}, μ_{ag} and v_{ag}) in Eqs. (10)–(18) should be replaced with K_{bk}, μ_{bk} and v_{bk} (K_F, μ_F and v_F), respectively. Secondly, K_F and μ_F should be turned into the effective bulk modulus and shear modulus of the three phase composite, denoted by K_S and μ_S, respectively. Thirdly, ϕ_{ag} should be replaced by ϕ_F, which can be defined by Eq. (19) as below.

$$\phi_F = \frac{c_{ag} + c_{itz}}{c_{ag} + c_{itz} + c_{bk}} \quad (19)$$

After performing the above modifications and replacing Eq. (18) with Eq. (19), the effective properties of the first equivalent matrix (which is concrete) made up of the aggregates, the ITZ and the bulk cement paste can be quantitatively reached with the second level homogenization.

4.4. The homogenization for the HFRC

There are usually two or more than two kinds of fibers, such as the steel fiber, polypropylene fiber and carbon fiber, in the HFRC. The different fibers are taken into considerations by averaging the lower bounds and upper bounds of the Halpin-Tsai model [75]. Take the steel fiber as the first type inclusion. The second equivalent matrix can be reached through homogenization of two-phase composite made up by the first equivalent matrix and the steel fiber inclusion. According to [30,75,76], the lower and upper bounds for the effective properties of the steel fiber reinforced concrete (the second equivalent matrix) can be expressed as follows:

$$K_{T1}^l = K_S\frac{1 + \xi_{k1}\eta_{k1}\phi_{st}}{1 - \eta_{k1}\phi_{st}}, \quad K_{T1}^u = K_S\frac{1 + \xi_{ku}\eta_{ku}\phi_{st}}{1 - \eta_{ku}\phi_{st}} \quad (20)$$

$$\mu_{T1}^l = \mu_S\frac{1 + \xi_{\mu1}\eta_{\mu1}\phi_{st}}{1 - \eta_{\mu1}\phi_{st}}, \quad \mu_{T1}^u = \mu_S\frac{1 + \xi_{\mu u}\eta_{\mu u}\phi_{st}}{1 - \eta_{\mu u}\phi_{st}} \quad (21)$$

$$\eta_{k1} = \frac{K_{st}/K_S - 1}{K_{st}/K_S + \xi_{k1}}, \quad \eta_{ku} = \frac{K_{st}/K_S - 1}{K_{st}/K_S + \xi_{ku}} \quad (22)$$

$$\eta_{\mu 1}=\frac{\mu_{st}/\mu_S-1}{\mu_{st}/\mu_S+\xi_{\mu 1}},\quad \eta_{\mu u}=\frac{\mu_{st}/\mu_S-1}{\mu_{st}/\mu_S+\xi_{\mu u}} \tag{23}$$

$$\xi_{k1}=\frac{\mu_S}{K_S},\quad \xi_{ku}=\frac{\mu_{st}}{K_S} \tag{24}$$

$$\xi_{\mu 1}=\frac{K_S}{2\mu_S+K_S},\quad \xi_{\mu u}=\frac{\mu_{st}K_{st}}{\mu_S(K_{st}+2\mu_{st})} \tag{25}$$

$$\phi_{st}=\frac{c_{\mathrm{st}}}{c_{\mathrm{ag}}+c_{\mathrm{itz}}+c_{\mathrm{bk}}+c_{\mathrm{st}}} \tag{26}$$

where K_{st}, μ_{st} and c_{st} represent the bulk modulus, shear modulus, and volume fraction of the steel fiber, respectively. K^l_{T1} and μ^l_{T1} (K^u_{T1} and μ^u_{T1}) are the lower bounds (upper bounds) for the effective bulk modulus and shear modulus of the second equivalent matrix. In this paper, the average of these two bounds are adopted as the estimations of the effective properties of the steel fiber reinforced concrete (the second equivalent matrix), which can be expressed as follows:

$$K_{T1}=\frac{1}{2}\left(K^l_{T1}+K^u_{T1}\right) \tag{27}$$

$$\mu_{T1}=\frac{1}{2}\left(\mu^l_{T1}+\mu^u_{T1}\right) \tag{28}$$

where K_{T1} and μ_{T1} are the effective bulk modulus and shear modulus of the second equivalent matrix.By updating the fiber type and

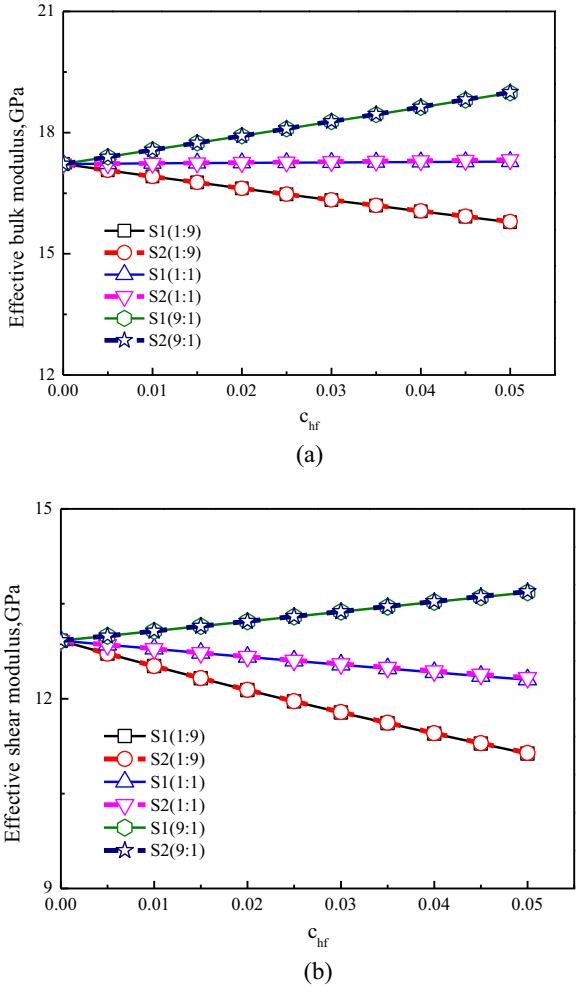

Fig. 3. The influence of homogenization sequences on the effective properties of HFRC, with S1 representing the first homogenization sequence which is to perform the former and the latter homogenizations with the steel fiber and the polypropylene fiber, respectively; with S2 representing the opposite sequence and ratio in the bracket denoting the volume proportions between the steel fiber and the polypropylene fiber. Here c_{hf} represent the sum of the two different fiber volume fractions.

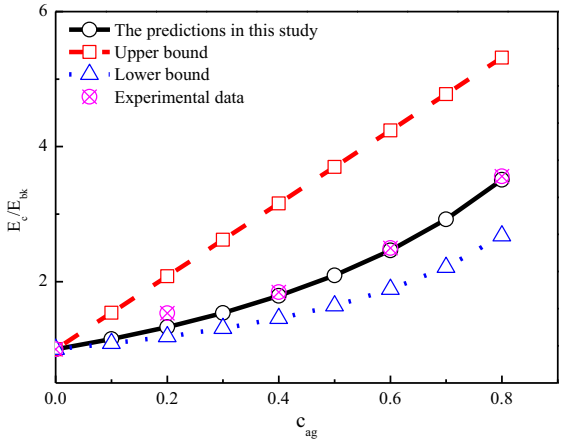

Fig. 4. Comparisons among our predictions, the existing micromechanical results and the experimental data [78] for the properties of concrete. Here c_{ag} is the volume fraction of the aggregates.

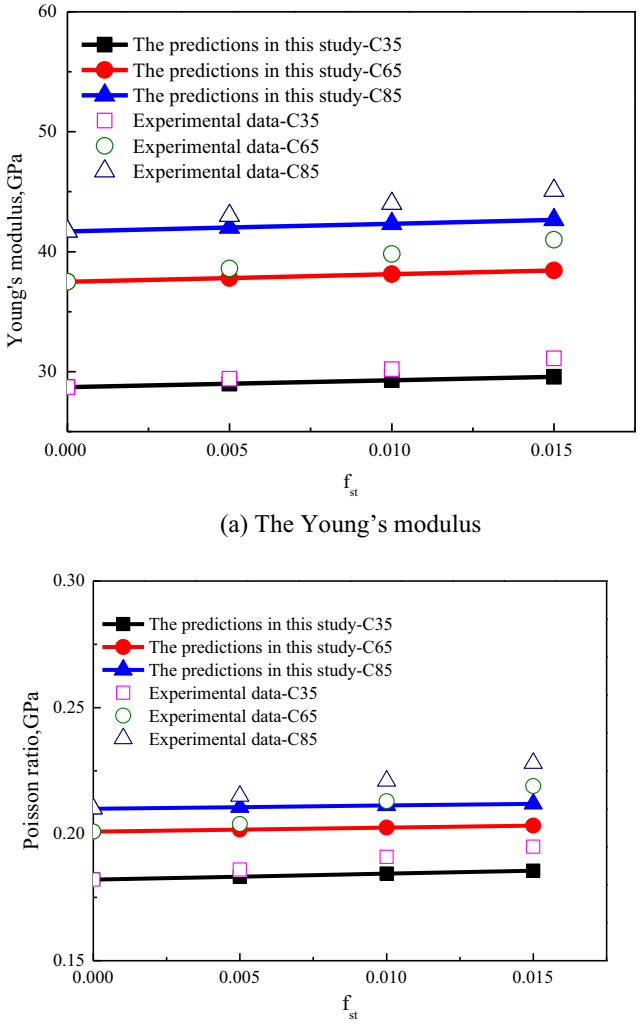

Fig. 5. Comparisons between the predictions in this study and the experimental data [13] for the properties of fiber reinforced concrete. Here f_{st} is the volume fraction of the fiber reinforced concrete.

the matrix phase, the other types of fiber can be similarly considered with Eqs. (20)–(28). Suppose that the polypropylene fiber is the ith kind of fiber in the HFRC. Let E_{po} and μ_{po} (E_{Ti} and μ_{Ti}) signify the bulk modulus and shear modulus of the polypropylene fiber (the ith equivalent matrix), respectively. The effective bulk modulus K_{Ti+1} and shear modulus μ_{Ti+1} of the $(i+1)$th equivalent matrix can be calculated through following modifications to Eqs. (20)–(28): (1) E_{st} and μ_{st} (E_S and μ_S) should be replaced by E_{po} and μ_{po} (E_{Ti} and μ_{Ti}), respectively. (2) E_{T1} and μ_{T1} should be replaced by E_{Ti+1} and μ_{Ti+1}, respectively. (3) Eq. (26) should be replaced by the volume fraction of the polypropylene fiber in the $(i+1)$th equivalent matrix, denoted by ϕ_{po}, which can be expressed as below:

$$\phi_{po} = \frac{c_{\mathrm{po}}}{c_{\mathrm{ag}} + c_{\mathrm{itz}} + c_{\mathrm{bk}} + c_{\mathrm{st}} + \cdots c_{i-1} + c_{\mathrm{po}}} \tag{29}$$

where c_{i-1} and c_{po} are the volume fractions of $(i-1)$th fiber and polypropylene fiber in the HFRC. If there are n kinds of fibers, the properties of the HFRC can be similarly calculated by the $(n+2)$th level homogenization.

4.5. Identification for the homogenization sequences for different types of fibers

Take the HFRC reinforced by the steel and polypropylene fiber as example. There are two homogenization sequences. One is to perform the former and latter homogenization with the steel fiber and the polypropylene fiber, respectively; the other is the opposite order.

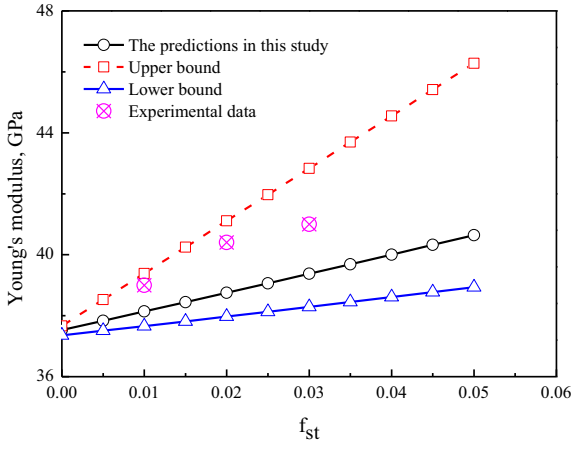

Fig. 6. Comparisons among our predictions, the existing micromechanical results and the experimental data [79] for the properties of HFRC with steel fiber and polypropylene fiber, where f_{st} is the volume fraction of the steel fiber, the volume fraction of polypropylene fiber is 0.11% in this example.

To investigate the influence of proportions of these two fibers on results obtained by different homogenization sequences, three kinds of volume ratios, including $c_{\mathrm{st}} : c_{\mathrm{po}} = 9{:}1$, 1:1 and 1:9, are employed as examples in this section. The experimental data of Williamson [77] are utilized as the input for the properties of the concrete and steel fiber. Specifically, the Young's modulus and Poisson's ratio of concrete (steel fiber) are 20.8 GPa (200 GPa) and 0.28 (0.3), respectively. These two constants of Polypropylene fiber are 4 GPa and 0.30 according to Dutra et al. [29]. It is noted that the properties of the concrete are those of the first equivalent matrix in the proposed framework.

Fig. 3(a) displays the variations in the effective bulk modulus of the HFRC with different inclusion volume fractions using two different homogenization sequences. c_{hf} means the sum of c_{st} and c_{po}. It can be observed that the predicted results are very near to each other with different homogenization sequences when different inclusion volume proportions are considered.

Similar conclusions can be reached as to the effective shear modulus as exhibited in Fig. 3(b), which implies that the homogenization sequence play little role in the predicted results herein, i.e. the proposed homogenization framework demonstrates adequate consistency and stability for predicting results with different homogenization sequences.

5. Verification and discussion

5.1. Comparison with the experimental data and results of the existing models

Both the experimental data and the existing micromechanical models are utilized to verify the proposed micromechanical model for the HFRC. The experimental data include mechanical properties of concrete [78], FRC [13] and HFRC [79,80].

Firstly, the Voigt upper bound and Reuss lower bound combined with the experimental data of [79] are employed to compare with the results obtained by the first and second level homogenizations, which are the predictions for the properties of the normal concrete made up of the aggregate, ITZ and cement paste. In their experiment, the maximum and minimum aggregate diameters were 19 and 0.15 mm, respectively, and the aggregate volume fraction was from 0.2 to 0.8. The Young's moduli of aggregate and neat cement paste were 74.5 and 11.6 GPa. As exhibited by Fig. 4, the predictions herein correspond well with the experimental data obtained by the Stock et al. [78]. Meanwhile the predictions lie reasonably between the Voigt upper bounds and Reuss lower bounds.

Secondly, the experimental data of Thomas and Ramaswamy [13] are adopted to illustrate the capacity of the proposed micromechanical framework to predict the properties of FRC. There are three types concrete matrix in their experiment, which are C35, C65 and C85, respectively. The volume fraction of the steel fiber varies from 0 to 1.5%, whose Young's modulus and Poisson's

Table 1
The predicted and experimental elastic moduli of HFRC, with E^* and E_0 representing the Young's modulus of the HFRC and the concrete matrix.

Steel fiber Volume Fraction, %	Palm fiber Volume Fraction, %	Synthetic fiber Volume Fraction, %	E^*/E_0			
			Experimental [80]	Reuss Lower bound	Voigt Upper bound	The predictions in this study
2.0	0	0	1.04	1.02	1.06	1.03
1.75	0.25	0	1.14	1.00	1.05	1.01
1.50	0.5	0	1.06	0.98	1.04	1.00
1.25	0.75	0	1.00	0.96	1.03	0.99
1.0	1.0	0	0.97	0.95	1.02	0.98
1.5	0.25	0.25	1.19	0.98	1.04	1.00
1.25	0.50	0.25	1.09	0.97	1.03	0.99
1.25	0.25	0.50	1.03	0.97	1.03	0.99
1.0	0.50	0.50	0.83	0.96	1.02	0.99

ratio are 210,000 MPa and 0.3, respectively. Fig. 5 shows the comparisons between the predictions herein and the experimental data for the properties of FRC. It can be found from Fig. 5(a) that the predicted Young's modulus for the FRC meet well with the experimental data when different types of concrete matrix are considered. Similar conclusions can be obtained for the effective Poisson's ratio reached by the proposed micromechanical framework, which is shown in Fig. 5(b).

Thirdly, to validate the presented micromechanical model for the HFRC, the experimental results of [79] are employed, where the steel fiber and polypropylene fiber are used. The volume fraction for the steel fiber varies from 1% to 3% and the volume fraction

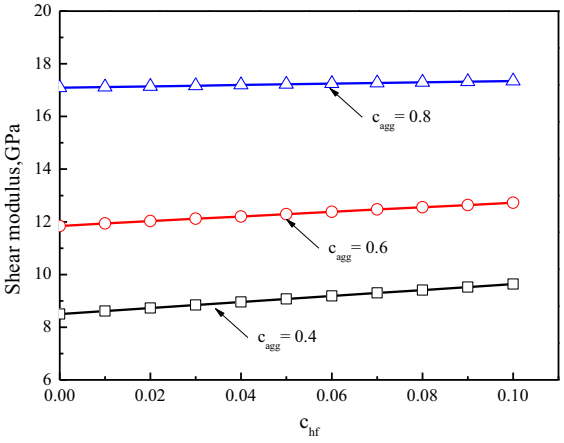

(a) The influence of the aggregate volume fraction on the shear modulus of HFRC

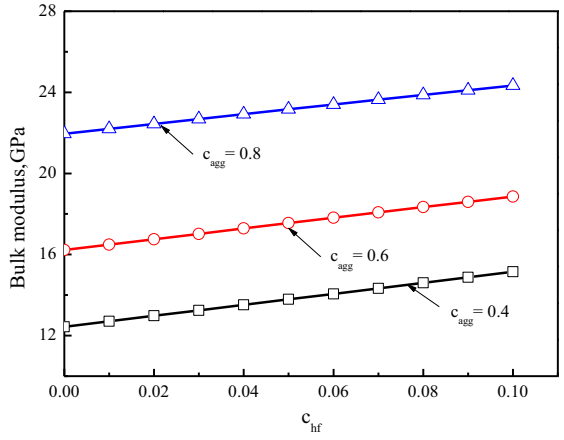

(b) The influence of the aggregate volume fraction on the bulk modulus of HFRC

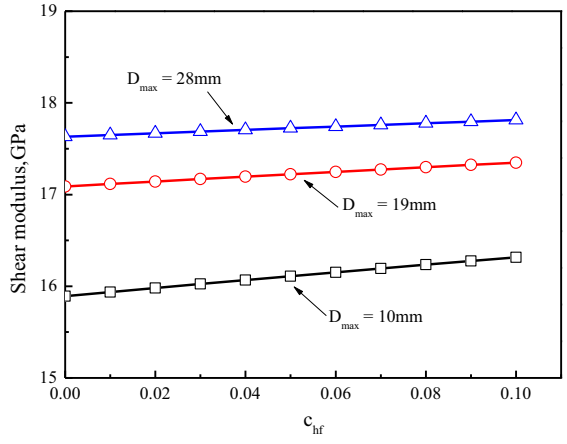

(c) The influence of the aggregate maximum diameter on the shear modulus of HFRC

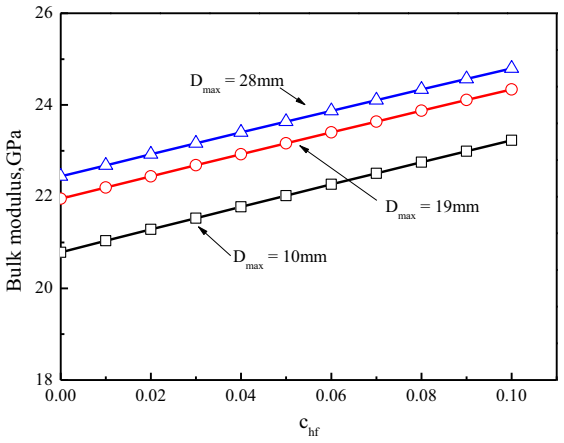

(d) The influence of the aggregate maximum diameter on the bulk modulus of HFRC

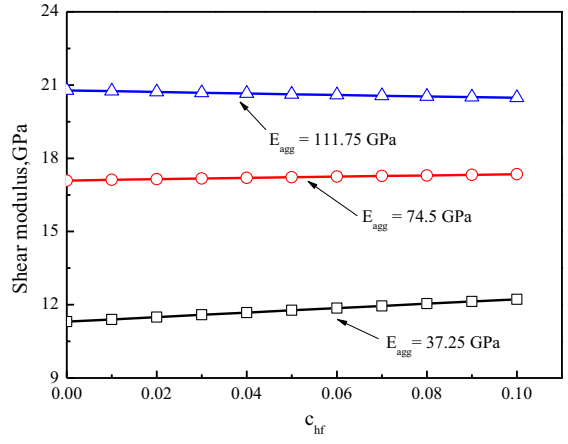

(e) The influence of the aggregate properties on the shear modulus of HFRC

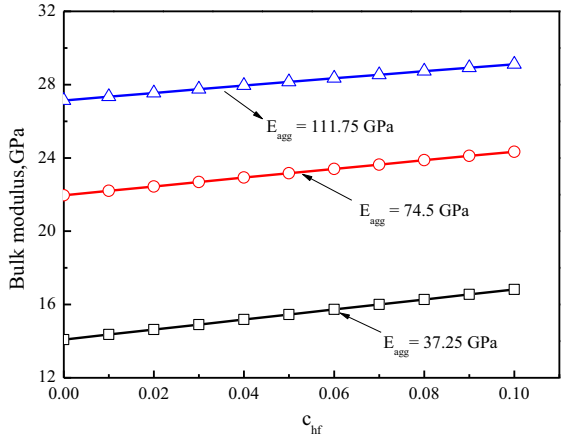

(f) The influence of the aggregate properties on the bulk modulus of HFRC

Fig. 7. The influence of the aggregate on the properties of HFRC, where c_{hf} is the sum of volume fractions of steel fiber and polypropylene fiber, the volume fraction ratio between them is 4:1.

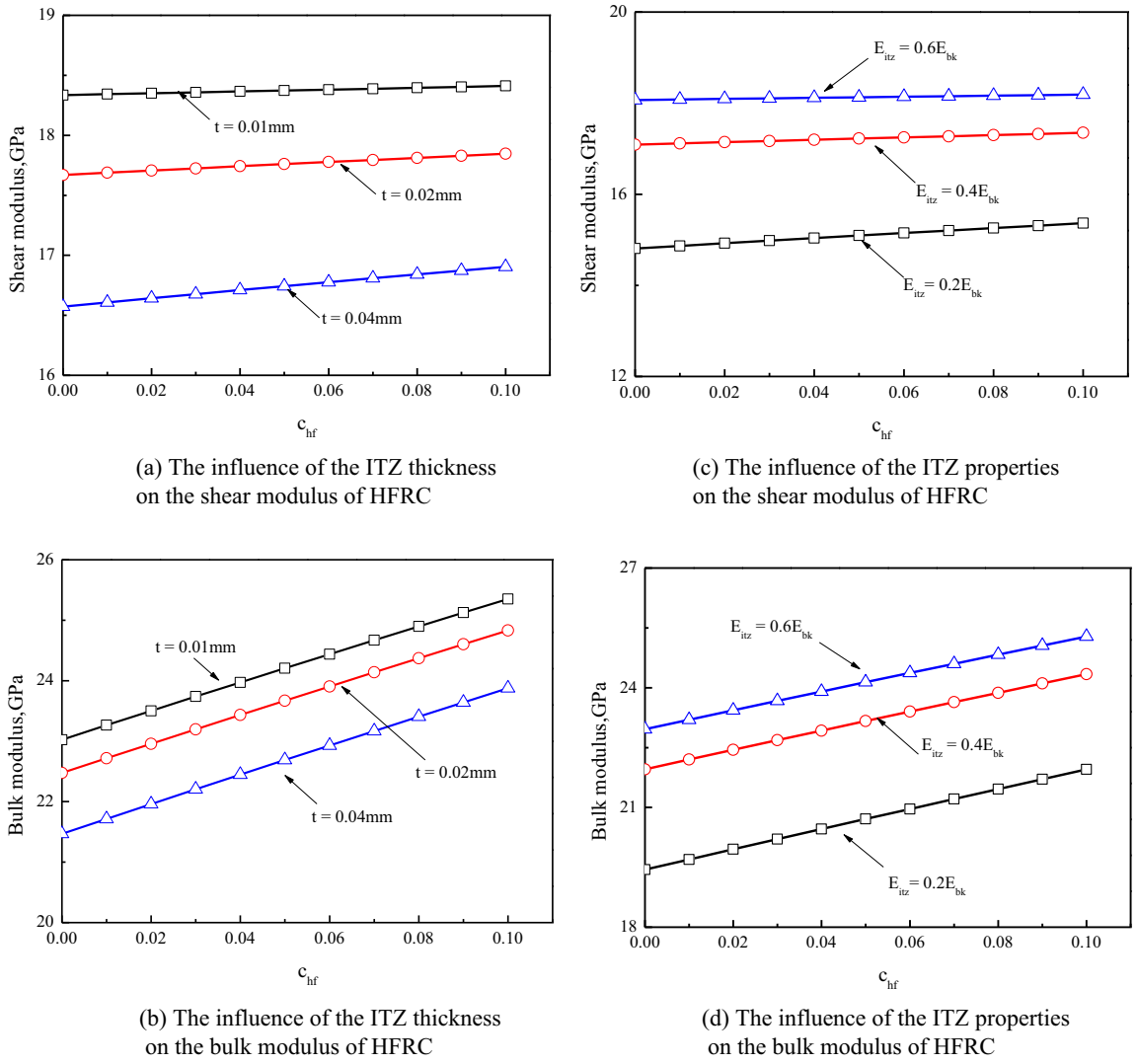

Fig. 8. The influence of the ITZ on the properties of HFRC, where c_{hf} is the sum of volume fractions of steel fiber and polypropylene fiber, the volume fraction ratio between them is 4:1.

for the polypropylene fiber is 0.11%. Meanwhile Dawood and Ramli's work [80], including the steel fiber, Palm fiber and Synthetic fiber, is also utilized to verify the presented micromechanical predictions. Fig. 6 shows the comparisons among the predictions of the proposed model, the existing micromechanical results and the experimental data for the properties of HFRC. From Fig. 6, it can observed that the predicted Young's modulus meet well with the experimental data of [79], with the maximum relative difference being 5%. Further, the predictions herein still stay between the two bounds reasonably.

When three different kinds of fibers are considered, the predictions herein are compared with the Voigt upper bound, Reuss lower bound and the experimental data of Dawood and Ramli [80], which is presented in Table 1. The results of the proposed model agree well with the experimental data, with the average relative difference being 3% and the maximum relative difference being 19%. At the same time, the results herein are still greater (lesser) than the lower bounds (the upper bounds) reasonably.

From the above, it can be summarized that the proposed micromechanical framework in this study is capable of predicting the properties of HFRC, FRC and concrete.

5.2. Influences of the aggregate and ITZ on the performance of the HFRC

The aggregate and ITZ have significant effects on the effective properties of the composite. To investigate these effects quantitatively, the steel fiber and polypropylene fiber are taken as examples and the volume fraction ratio between them is 4:1. The properties of the aggregate, ITZ, and the cement paste in [78] are taken as the inputs for the numerical simulations.

Fig. 7(a) and (b) display the influence of aggregate volume fraction on the shear modulus and bulk modulus of HFRC. It can be found that the properties of the composite increase and the enhancement of fibers become less when the volume fraction of the aggregate increase.

The different maximum diameter of the aggregate will lead to different volume fractions of the ITZ, which will influence the properties of HFRC, even though the volume fractions are the same. Fig. 7(c) and (d) demonstrate the influence of the aggregate maximum diameter. In this example, the aggregate volume fraction is 0.8 and the fuller grading is considered. It can be observed that the shear modulus and bulk modulus of the composite become greater with the increase of the aggregate diameter.

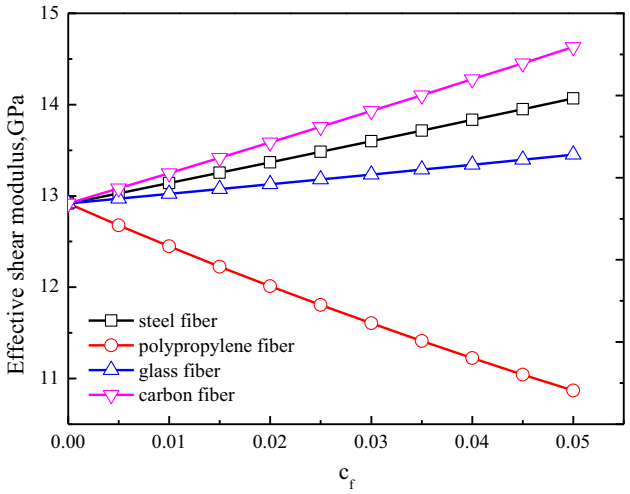

(a) The effective shear modulus

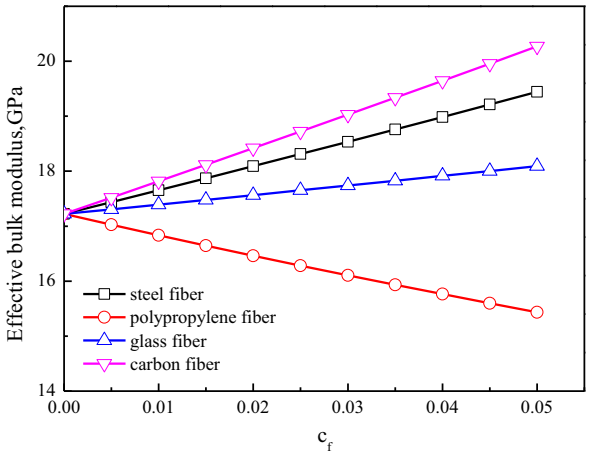

(b) The effective bulk modulus

Fig. 9. The influence of the fibers on the properties of FRC, where c_f is the volume fraction of different fibers.

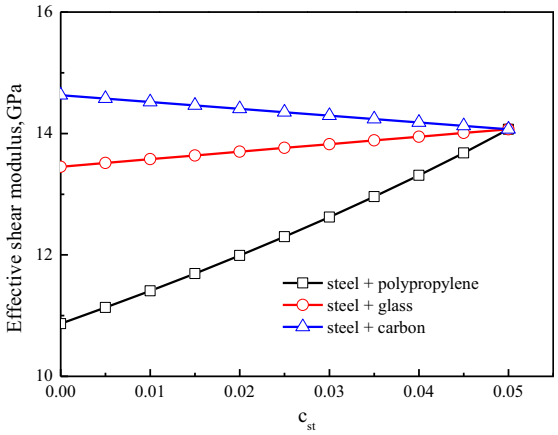

(a) The effective shear modulus

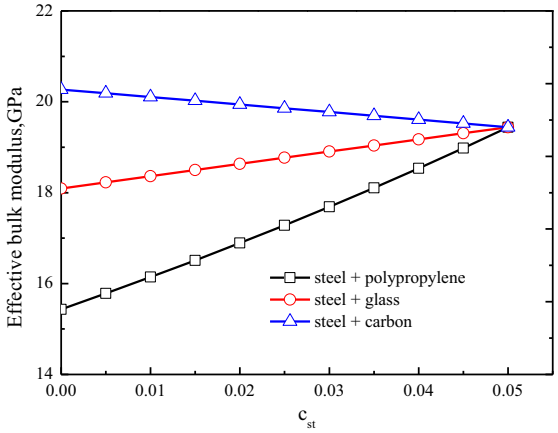

(b) The effective bulk modulus

Fig. 10. The influence of the fiber mix proportions on the properties of HFRC, where c_{st} is the volume fraction of steel fiber. The volume fraction of each hybrid fibers is 5%.

The higher properties of the aggregate may lead to stronger properties of HFRC, which is shown by Fig. 7(e) and (f) for the shear modulus and bulk modulus, respectively.

Fig. 8 shows the effects of the ITZ on the properties of HFRC. It is noted that the exact value of the ITZ thickness is not the focus in this study. More attention is paid to the quantitative influence of the ITZ on the properties of HFRC for a given thickness. Suppose that the volume fraction and properties of aggregate and the fibers are constant, the properties of HFRC reduce with the increase of ITZ thickness, as exhibited in Fig. 8(a) and (b). From Fig. 8(c) and (d), it can be found that with the increase of the ITZ properties, the composite demonstrates stronger properties.

5.3. Influences of the fiber types, concentrations and mix proportions on the performance of the HFRC

Four different types of fibers, including steel, carbon, polypropylene and glass fiber, are employed to illustrate the influences of fiber types and concentrations on the performance of FRC. Fig. 9 shows variations of the effective properties of FRC when different fibers are considered. It can be seen from Fig. 9(a) that the carbon fiber reinforced concrete (CFRC) demonstrates the highest shear modulus and the fibers improve mechanical properties of the concrete matrix better with the increase of their volume fraction. Similar trend can be found in Fig. 9(b) for the bulk modulus of FRC.

Three types of hybrid fibers are employed as examples to consider the influence of their mix proportions on the performance of the HFRC. The polypropylene, glass and carbon fiber are respectively mixed with steel fiber as the first, second and third type of hybrid fibers. The total volume fraction of each hybrid fibers is 5% as constant. Fig. 10(a) and (b) present the variations in the mechanical properties of the HFRC when different fiber mix proportions are considered. Due to the high properties of the steel and carbon fiber, the combination of these two fibers improves the shear modulus and bulk modulus best. Because the properties of the steel fiber are stronger than those of glass and polypropylene fiber, with the increase of the steel fiber, the HFRC's mechanical performance improves when the first and second type hybrid fibers are considered. However, since the carbon fiber's properties are higher than those of the steel fiber, the HFRC's properties decrease when the relative volume fraction of steel fiber increases as to the third type hybrid fibers.

6. Conclusions

As an extension of the previous micromechanical model for FRC, this paper presents a multiphase micromechanical model for HFRC considering the aggregate and ITZ effects. In the proposed model,

HFRC is seen as a multiphase composite composed of the aggregates, ITZ, bulk cement paste and different types of fibers. The volume fraction of the ITZ is analytically calculated according to the aggregate grading. A new multi-level homogenization schemes based on the generalized self-consistent approach and the Halpin-Tsai model are developed to predict the effective properties of HFRC. The first equivalent matrix, known as concrete, are obtained with the first and second level homogenization procedures to the composite composed by the aggregate, cement paste and the ITZ between them. The properties of HFRC are reached using the multi-level homogenization process through adding different types of fibers step by step into the equivalent matrix. Moreover, the predicted results herein are compared to available experimental data and the existing estimations. The influences of the aggregate, ITZ and fibers on the properties of HFRC are discussed.

From this study, the following main conclusions can be drawn:

(1) The proposed multi-phase micromechanical framework for HFRC is capable of predicting the properties of the HFRC with the aggregate and ITZ effects. For the special cases, the properties of concrete and FRC can also be calculated by the presented micromechanical models in this study.
(2) The quantitative effects of the maximum size, the volume fraction and properties of aggregates on the HFRC's effective properties can be predicted with the proposed micromechanical framework. Meanwhile, the influence of ITZ on the mechanical performance of the HFRC can be estimated for a given ITZ thicknesses. However, it is noted that the exact value for the ITZ thickness is not considered in this study.
(3) Based on the proposed model in this study, the moduli of HFRC can be best improved by the carbon fiber, which is followed by the steel fiber, glass fiber and polypropylene fiber. The effects of different types of fibers can be quantitatively taken into considerations by the multi-level homogenization scheme step by step. However, the homogenization sequence for different fibers has little influence on the predicting results herein.

Acknowledgements

This work is supported by the National Natural Science Foundation of China (51508404, 51578410). This work is also supported by Shanghai Pujiang Program (14PJD034), Key Laboratory of Advanced Civil Engineering Materials (Tongji University), Ministry of Education, 1000 Talents Plan Short-Term Program by the Organization Department of the Central Committee of the CPC, the Fundamental Research Funds for the Central Universities (Tongji University), the youth talents training plan of Tongji University, Research Program of State Key Laboratory for Disaster Reduction in Civil Engineering, and the Scientific Platform Open Funds of Fundamental Research Plan for the Central Universities, Chang'an University (310821151113).

Appendix A

There are two homogenization sequences to obtain the effective properties of the HFRC reinforced by the steel fiber and polypropylene fiber. For the first sequence, the lower and upper bounds for the properties of the second equivalent matrix composed by the concrete and the steel fiber can be obtained as below [22,67,68]:

$$K_{T1}^{l}=K_S\frac{1+\xi_{k1}\eta_{k1}\phi_{st}}{1-\eta_{k1}\phi_{st}},\quad K_{T1}^{u}=K_S\frac{1+\xi_{ku1}\eta_{ku1}\phi_{st}}{1-\eta_{ku1}\phi_{st}} \tag{A1}$$

$$\mu_{T1}^{l}=\mu_S\frac{1+\xi_{\mu1}\eta_{\mu1}\phi_{st}}{1-\eta_{\mu1}\phi_{st}},\quad \mu_{T1}^{u}=\mu_S\frac{1+\xi_{\mu u1}\eta_{\mu u1}\phi_{st}}{1-\eta_{\mu u1}\phi_{st}} \tag{A2}$$

$$\eta_{k1}=\frac{K_{st}/K_S-1}{K_{st}/K_S+\xi_{k1}},\quad \eta_{ku1}=\frac{K_{st}/K_S-1}{K_{st}/K_S+\xi_{ku1}} \tag{A3}$$

$$\eta_{\mu1}=\frac{\mu_{st}/\mu_S-1}{\mu_{st}/\mu_S+\xi_{\mu1}},\quad \eta_{\mu u1}=\frac{\mu_{st}/\mu_S-1}{\mu_{st}/\mu_S+\xi_{\mu u}} \tag{A4}$$

$$\xi_{k1}=\frac{\mu_S}{K_S},\quad \xi_{ku1}=\frac{\mu_{st}}{K_S} \tag{A5}$$

$$\xi_{\mu1}=\frac{K_S}{2\mu_S+K_S},\quad \xi_{\mu u1}=\frac{\mu_{st}K_{st}}{\mu_S(K_{st}+2\mu_{st})} \tag{A6}$$

$$\phi_{st}=\frac{c_{\mathrm{st}}}{c_{\mathrm{ag}}+c_{\mathrm{itz}}+c_{\mathrm{bk}}+c_{\mathrm{st}}} \tag{A7}$$

where K_{st}, μ_{st} and c_{st} represent the bulk modulus, shear modulus, and volume fraction of the steel fiber, respectively. K_{T1}^{l} and μ_{T1}^{l} (K_{T1}^{u} and μ_{T1}^{u}) are the lower bounds (upper bounds) for the effective bulk modulus and shear modulus of the second equivalent matrix. In this paper, the average of these two bounds are adopted as the estimations of the effective properties of the steel fiber reinforced concrete (the second equivalent matrix), which can be expressed as follows

$$K_{T1}^{F}=\frac{1}{2}\left(K_{T1}^{l}+K_{T1}^{u}\right) \tag{A8}$$

$$\mu_{T1}^{F}=\frac{1}{2}\left(\mu_{T1}^{l}+\mu_{T1}^{u}\right) \tag{A9}$$

where K_{T1}^{F} and μ_{T1}^{F} are the effective bulk modulus and shear modulus of the second equivalent matrix using the first homogenization sequence. The properties of the HFRC can be similarly reached as below:

$$K_{T2}^{F}=\frac{1}{2}\left(K_{T2}^{l}+K_{T2}^{u}\right) \tag{A10}$$

$$\mu_{T2}^{F}=\frac{1}{2}\left(\mu_{T2}^{l}+\mu_{T2}^{u}\right) \tag{A11}$$

With

$$K_{T2}^{l}=K_{T1}^{F}\frac{1+\xi_{k2}\eta_{k2}\phi_{po}}{1-\eta_{k2}\phi_{po}},\quad K_{T2}^{u}=K_{T1}^{F}\frac{1+\xi_{ku2}\eta_{ku2}\phi_{po}}{1-\eta_{ku2}\phi_{po}} \tag{A12}$$

$$\mu_{T2}^{l}=\mu_{T1}^{F}\frac{1+\xi_{\mu2}\eta_{\mu2}\phi_{po}}{1-\eta_{\mu2}\phi_{po}},\quad \mu_{T2}^{u}=\mu_{T1}^{F}\frac{1+\xi_{\mu u2}\eta_{\mu u2}\phi_{po}}{1-\eta_{\mu u2}\phi_{po}} \tag{A13}$$

$$\eta_{k2}=\frac{K_{po}/K_{T1}^{F}-1}{K_{po}/K_{T1}^{F}+\xi_{k2}},\quad \eta_{ku2}=\frac{K_{po}/K_{T1}^{F}-1}{K_{po}/K_{T1}^{F}+\xi_{ku2}} \tag{A14}$$

$$\eta_{\mu2}=\frac{\mu_{po}/\mu_{T1}^{F}-1}{\mu_{po}/\mu_{T1}^{F}+\xi_{\mu2}},\quad \eta_{\mu u2}=\frac{\mu_{po}/\mu_{T1}^{F}-1}{\mu_{po}/\mu_{T1}^{F}+\xi_{\mu u2}} \tag{A15}$$

$$\xi_{k2}=\frac{\mu_{T1}^{F}}{K_{T1}^{F}},\quad \xi_{ku}=\frac{\mu_{po}}{K_{T1}^{F}} \tag{A16}$$

$$\xi_{\mu2}=\frac{K_{T1}^{F}}{2\mu_{T1}^{F}+K_{T1}^{F}},\quad \xi_{\mu u2}=\frac{\mu_{po}K_{po}}{\mu_{T1}^{F}(K_{po}+2\mu_{po})} \tag{A17}$$

$$\phi_{po}=\frac{c_{po}}{c_{\mathrm{ag}}+c_{\mathrm{itz}}+c_{\mathrm{bk}}+c_{\mathrm{st}}+c_{po}} \tag{A18}$$

where K_{T2}^F and μ_{T2}^F are the effective bulk modulus and shear modulus of the HFRC using the first homogenization sequence.

As to the second homogenization sequence, the properties of the second equivalent matrix composed by the concrete and the polypropylene fiber can be obtained similarly as below [22,67,68]:

$$K_{T1}^S = \frac{1}{2}\left(K_{T1}^l + K_{T1}^u\right) \tag{A19}$$

$$\mu_{T1}^S = \frac{1}{2}\left(\mu_{T1}^l + \mu_{T1}^u\right) \tag{A20}$$

With

$$K_{T1}^l = K_S\frac{1+\xi_{k1}\eta_{k1}\phi_{po}}{1-\eta_{k1}\phi_{po}}, \quad K_{T1}^u = K_S\frac{1+\xi_{ku1}\eta_{ku1}\phi_{po}}{1-\eta_{ku1}\phi_{po}} \tag{A21}$$

$$\mu_{T1}^l = \mu_S\frac{1+\xi_{\mu1}\eta_{\mu1}\phi_{po}}{1-\eta_{\mu1}\phi_{po}}, \quad \mu_{T1}^u = \mu_S\frac{1+\xi_{\mu u1}\eta_{\mu u1}\phi_{po}}{1-\eta_{\mu u1}\phi_{po}} \tag{A22}$$

$$\eta_{k1} = \frac{K_{po}/K_S - 1}{K_{po}/K_S + \xi_{k1}}, \quad \eta_{ku1} = \frac{K_{po}/K_S - 1}{K_{po}/K_S + \xi_{ku1}} \tag{A23}$$

$$\eta_{\mu1} = \frac{\mu_{po}/\mu_S - 1}{\mu_{po}/\mu_S + \xi_{\mu1}}, \quad \eta_{\mu u1} = \frac{\mu_{po}/\mu_S - 1}{\mu_{po}/\mu_S + \xi_{\mu u}} \tag{A24}$$

$$\xi_{k1} = \frac{\mu_S}{K_S}, \quad \xi_{ku1} = \frac{\mu_{po}}{K_S} \tag{A25}$$

$$\xi_{\mu1} = \frac{K_S}{2\mu_S + K_S}, \quad \xi_{\mu u1} = \frac{\mu_{po}K_{st}}{\mu_S(K_{po} + 2\mu_{po})} \tag{A26}$$

$$\phi_{po} = \frac{c_{po}}{c_{ag} + c_{itz} + c_{bk} + c_{po}} \tag{A27}$$

where K_{T1}^S and μ_{T1}^S are the effective bulk modulus and shear modulus of the second equivalent matrix using the second homogenization sequence. The properties of the HFRC can be similarly calculated:

$$K_{T2}^S = \frac{1}{2}\left(K_{T2}^l + K_{T2}^u\right) \tag{A28}$$

$$\mu_{T2}^S = \frac{1}{2}\left(\mu_{T2}^l + \mu_{T2}^u\right) \tag{A29}$$

With

$$K_{T2}^l = K_{T1}^S\frac{1+\xi_{k2}\eta_{k2}\phi_{st}}{1-\eta_{k2}\phi_{st}}, \quad K_{T2}^u = K_{T1}^S\frac{1+\xi_{ku2}\eta_{ku2}\phi_{st}}{1-\eta_{ku2}\phi_{st}} \tag{A30}$$

$$\mu_{T2}^l = \mu_{T1}^S\frac{1+\xi_{\mu2}\eta_{\mu2}\phi_{st}}{1-\eta_{\mu2}\phi_{st}}, \quad \mu_{T2}^u = \mu_{T1}^S\frac{1+\xi_{\mu u2}\eta_{\mu u2}\phi_{st}}{1-\eta_{\mu u2}\phi_{st}} \tag{A31}$$

$$\eta_{k2} = \frac{K_{st}/K_{T1}^S - 1}{K_{st}/K_{T1}^S + \xi_{k2}}, \quad \eta_{ku2} = \frac{K_{st}/K_{T1}^S - 1}{K_{st}/K_{T1}^S + \xi_{ku2}} \tag{A32}$$

$$\eta_{\mu2} = \frac{\mu_{st}/\mu_{T1}^S - 1}{\mu_{st}/\mu_{T1}^S + \xi_{\mu2}}, \quad \eta_{\mu u2} = \frac{\mu_{st}/\mu_{T1}^S - 1}{\mu_{st}/\mu_{T1}^S + \xi_{\mu u2}} \tag{A33}$$

$$\xi_{k2} = \frac{\mu_{T1}^S}{K_{T1}^S}, \quad \xi_{ku} = \frac{\mu_{st}}{K_{T1}^S} \tag{A34}$$

$$\xi_{\mu2} = \frac{K_{T1}^S}{2\mu_{T1}^S + K_{T1}^S}, \quad \xi_{\mu u2} = \frac{\mu_{st}K_{st}}{\mu_{T1}^S(K_{st} + 2\mu_{st})} \tag{A35}$$

$$\phi_{st} = \frac{c_{st}}{c_{ag} + c_{itz} + c_{bk} + c_{st} + c_{po}} \tag{A36}$$

where K_{T2}^S and μ_{T2}^S are the effective bulk modulus and shear modulus of the HFRC using the second homogenization sequence.

References

[1] Y. Mohammadi, R. Carkon-Azad, S.P. Singh, S.K. Kaushik, Impact resistance of steel fibrous concrete containing fibres of mixed aspect ratio, Constr. Build. Mater. 23 (2009) 183–189.
[2] P. Di Maida, E. Radi, C. Sciancalepore, et al., Pullout behavior of polypropylene macro-synthetic fibers treated with nano-silica, Constr. Build. Mater. 85 (2015) 39–44.
[3] Y.S. Zhang, W. Sun, Z.J. Li, et al., Impact properties of geopolymer based extrudates incorporated with fly ash and PVA short fiber, Constr. Build. Mater. 22 (3) (2008) 370–383.
[4] N. Buratti, B. Ferracuti, M. Savoia, Concrete crack reduction in tunnel linings by steel fibre-reinforced concretes, Constr. Build. Mater. 44 (2013) 249–259.
[5] M. Mandhkan, R. Azizkhani, M.E.T. Harchegani, Effects of pozzolans together with steel and polypropylene fibers on mechanical properties of RCC pavements, Constr. Build. Mater. 26 (2012) 102–112.
[6] M.N. Soutsos, T.T. Le, A.P. Lampropoulos, Flexural performance of fibre reinforced concrete made with steel and synthetic fibre, Constr. Build. Mater. 36 (2012) 704–710.
[7] S. Yazıcı, G. Inan, V. Tabak, Effect of aspect ratio and volume fraction of steel fiber on the mechanical properties of SFRC, Constr. Build. Mater. 21 (2007) 1250–1253.
[8] F. Köksal, F. Altun, İ. Yiğit, Y. Sahin, Combined effect of silica fume and steel fiber on the mechanical properties of high strength concretes, Constr. Build. Mater. 22 (2008) 1874–1880.
[9] F. Altun, T. Haktanir, K. Ari, Effects of steel fiber addition on mechanical properties of concrete and RC beams, Constr. Build. Mater. 21 (2007) 654–661.
[10] Z.G. Yan, H.H. Zhu, J.W. Ju, Behavior of reinforced concrete and steel fiber reinforced concrete shield TBM tunnel linings exposed to high temperatures, Constr. Build. Mater. 38 (2013) 610–618.
[11] C.D. Atis, O. Karahan, Properties of steel fiber reinforced fly ash concrete, Constr. Build. Mater. 23 (2009) 392–399.
[12] B. Felekoglu, S. Turkel, Y. Altuntas, Effects of steel fiber reinforcement on surface wear resistance of self- compacting repair mortars, Cem. Concr. Compos. 29 (2007) 391–396.
[13] J. Thomas1, A. Ramaswamy, Mechanical properties of steel fiber-reinforced concrete, J. Mater. Civ. Eng. 19 (2007) 385–392.
[14] A. Badr, A.F. Ashour, A.K. Platten, Statistical variations in impact resistance of polypropylene fiber-reinforced concrete, Int. J. Impact Eng 32 (2006) 1907–1920.
[15] M. Nili, V. Afroughsabet, The effects of silica fume and polypropylene fibers on the impact resistance and mechanical properties, Constr. Build. Mater. 24 (2010) 927–933.
[16] S.L. Shen, Z.F. Wang, J. Yang, E.C. Ho, Generalized approach for prediction of jet grout column diameter, J. Geotech. Geoenviron. 139 (12) (2013) 2060–2069.
[17] Z.F. Wang, S.L. Shen, E.C. Ho, Y.H. Kim, Investigation of field installation effects of horizontal twin-jet grouting in Shanghai soft soil deposits, Can. Geotech. J. 50 (3) (2013) 288–297.
[18] S.L. Shen, Z.F. Wang, W.J. Sun, L.B. Wang, S. Horpibulsuk, A field trial of horizontal jet grouting using the composite-pipe method in the soft deposit of Shanghai, Tunn. Undergr. Sp. Tech. 35 (2013) 142–151.
[19] S.L. Shen, Z.F. Wang, S. Horpibulsuk, Y.H. Kim, Jet-grouting with a newly developed technology: the twin-jet method, Eng. Geol. 152 (1) (2013) 87–95.
[20] Z.F. Wang, S.L. Shen, C.E. Ho, Y.S. Xu, Jet grouting for mitigation of installation disturbance, Proc. Inst. Civil Eng. Geotech. 167 (GE6) (2014) 526–536.
[21] M. Chen, S.L. Shen, A. Arulrajah, H.N. Wu, D.W. Hou, Y.S. Xu, Characteristics of strength development of fiber-reinforced and cement improved soft clay of Shanghai, Geotext. Geomembr. 43 (6) (2015) 515–523.
[22] N. Zhang, S.L. Shen, H.N. Wu, J.C. Chai, Z.Y. Yin, Evaluation of performance of embankments with reinforcement on PVD-improved marine clay, Geotext. Geomembr. 43 (6) (2015) 506–514.
[23] Z.F. Wang, S.L. Shen, Z.Y. Yin, Y.S. Xu, Rapid field evaluation of the strength of cement stabilized clayey soil, Bull. Eng. Geol. Environ. 74 (3) (2015) 991–999.
[24] K.H. Tan, P. Paramasivam, K.C. Tan, Instantaneous and long-term deflections of steel fiber reinforced concrete beams, ACI Struct. J. 91 (1994) 384–393.
[25] S.A. Ashour, F.F. Wafa, M.I. Kamal, Effect of concrete compressive strength and tensile reinforcement ratio on the flexural behavior of fibruous concrete beams, Eng. Struct. 22 (2000) 1145–1158.
[26] A.S. Ezeldin, P.N. Balagaru, Normal and high strength fiber reinforced concrete under compression, J. Mater. Civil Eng. 4 (1992) 415–429.
[27] M.A. Mansur, M.S. Chin, T.H. Wee, Stress–strain relationship of high strength fiber concrete in compression, J. Mater. Civil Eng. 11 (1999) 21–29.
[28] H.A. Ahmad, C.L. Lagoudas, Effective elastic properties of fiber-reinforced concrete with random fibers, J. Eng. Mech. 117 (1991) 2931–2938.
[29] V.F.P. Dutra, S. Maghous, A.C. Filho, A.R. Pacheco, A micromechanical approach to elastic and viscoelastic properties of fiber reinforced concrete, Cem. Concr. Res. 40 (2010) 460–472.

[30] T.L. Teng, Y.A. Chu, F.A. Chang, H.S. Chin, Calculating the elastic moduli of steel fiber reinforced concrete using a dedicated empirical formula, Comput. Mater. Sci. 31 (2004) 337–346.
[31] E. Gal, R. Kryvoruk, Meso-scale analysis of FRC using a two-step homogenization approach, Comput. Struct. 89 (2011) 921–929.
[32] X.F. Guan, X. Liu, X. Jia, Y. Yuan, J.Z. Cui, Mang HA.A stochastic multiscale model for predicting mechanical properties of fiber reinforced concrete, Int. J. Solids Struct. 56–57 (2015) 280–289.
[33] Z.G. Yan, Y. Shen, H.H. Zhu, Y. Lu, X.J. Li, Experimental investigation of reinforced concrete and hybrid fiber reinforced concrete shield tunnel segments subjected to elevated temperature, Fire Saf. J. 71 (2015) 86–99.
[34] P.S. Song, J.C. Wu, S. Hwang, B.C. Sheu, Statistical analysis of impact strength and strength reliability of steel-polypropylene hybrid fiber reinforced concrete, Constr. Build. Mater. 19 (2005) 1–9.
[35] B. Chen, J. Liu, Contribution of hybrid fibers on the properties of the high strength lightweight concrete having good workability, Cem. Concr. Res. 35 (2005) 913–917.
[36] E.T. Dawood, M. Ramli, High strength characteristics of cement mortar reinforced with hybrid fibres, Constr. Build. Mater. 25 (5) (2011) 2240–2247.
[37] B. Chen, J. Liu, Residual strength of hybrid-fiber-reinforced high-strength concrete after exposure to high temperatures, Cem. Concr. Res. 34 (2004) 1065–1069.
[38] Y. Mohammadi, S.P. Singh, S.K. Kaushik, Properties of steel fibrous concrete containing mixed fibrers in fresh and hardened state, Constr. Build. Mater. 29 (2008) 956–965.
[39] A. Sivakumar, M. Santhanam, Mechanical properties of high strength concrete reinforced with metallic and non-metallic fibers, Cem. Concr. Compos. 29 (2007) 603–608.
[40] E.T. Dawood, M. Ramli, Development of high strength flowable mortar with hybrid fiber, Constr. Build. Mater. 24 (2010) 1043–1050.
[41] O. Bernard, F.J. Ulm, E. Lemarchand, A multiscale micromechanics-hydration model for the early-age elastic properties of cement-based materials, Cem. Concr. Res. 33 (2003) 1293–1309.
[42] G. Constantinides, F.J. Ulm, The effect of two types of C–S–H on the elasticity of cement-based materials: results from nanoindentation and micromechanical modeling, Cem. Concr. Res. 34 (1) (2004) 67–80.
[43] J.J. Zheng, H.S. Wong, N.R. Buenfeld, Assessing the influence of ITZ on the steady-state chloride diffusivity of concrete using a numerical model, Cem. Concr. Res. 39 (2009) 805–813.
[44] J.J. Zheng, X.Z. Zhou, X.Y. Jin, An n-layered spherical inclusion model for predicting the elastic moduli of concrete with inhomogeneous ITZ, Cem. Concr. Compos. 34 (2012) 716–723.
[45] W. Dridi, Analysis of effective diffusivity of cement based materials by multi-scale modelling, Mater. Struct. 46 (2013) 313–326.
[46] K. Yanase, J.W. Ju, Effective elastic moduli of spherical particle reinforced composites containing imperfect interfaces, Int. J. Damage Mech. 21 (1) (2012) 97–127.
[47] Q. Chen, M. MousaviNezhad, Q. Fisher, H.H. Zhu, Multi-scale approach for modeling the transversely isotropic elastic properties of shale considering multi-inclusions and interfacial transition zone, Int. J. Rock. Mech. Min. 84 (2016) 95–104.
[48] E.J. Garboczi, D.P. Bentz, Analytical formulas for interfacial transition zone properties, Adv. Cem. Based Mater. 6 (3–4) (1997) 99–108.
[49] G.Q. Li, Y. Zhao, S.S. Pang, Four-phase sphere modeling of effective bulk modulus of concrete, Cem. Concr. Res. 29 (1999) 839–845.
[50] B.L. Lu, S. Torquato, Nearest-surface distribution functions for polydispersed particle system, Phys. Rev. A 45 (8) (1992) 5530–5544.
[51] S. Caré, E. Hervé, Application of a n-phase model to the diffusion coefficient of chloride in mortar, Transp. Porous Media 56 (2) (2004) 119–135.
[52] E.J. Garboczi, D.P. Bentz, Multiscale analytical/numerical theory of the diffusivity of concrete, Adv. Cem. Based Mater. 8 (1998) 77–88.
[53] J.W. Ju, T.M. Chen, Micromechanics and effective moduli of elastic composites containing randomly dispersed ellipsoidal inhomogeneities, Acta Mech. 103 (1994) 103–121.
[54] E.J. Garboczi, J.G. Berryman, Elastic moduli of a material containing composite inclusions: effective medium theory and finite element computations, Mech. Mater. 33 (2) (2001) 455–470.
[55] Q.S. Yang, X. Tao, H. Yang, A stepping scheme for predicting effective properties of the multi-inclusion composites, Int. J. Eng. Sci. 45 (2007) 997–1006.
[56] N.B. Nguyen, A. Giraud, D. Grgic, A composite sphere assemblage model for porous oolitic rocks, Int. J. Rock. Mech. Min. 48 (2011) 909–921.
[57] J.W. Ju, K. Yanase, Micromechanics and effective elastic moduli of particle-reinforced composites with near-field particle interactions, Acta Mech. 215 (1) (2010) 135–153.
[58] J.W. Ju, K. Yanase, Micromechanical effective elastic moduli of continuous fiber-reinforced composites with near-field fiber interactions, Acta Mech. 216 (1) (2011) 87–103.
[59] J.W. Ju, T.M. Chen, Effective elastic moduli of two-phase composites containing randomly dispersed spherical inhomogeneities, Acta Mech. 103 (1994) 123–144.
[60] J.W. Ju, X.D. Zhang, Micromechanics and effective transverse elastic moduli of composites with randomly located aligned circular fibers, Int. J. Solids Struct. 35 (9–10) (1998) 941–960.
[61] J.W. Ju, L.Z. Sun, A novel formulation for the exterior-point Eshelby's tensor of an ellipsoidal inclusion, J. Appl. Mech-T ASME 66 (2) (1999) 570–574.
[62] J.W. Ju, L.Z. Sun, Effective elastoplastic behavior of metal matrix composites containing randomly located aligned spheroidal inhomogeneities. Part I: micromechanics-based formulation, Int. J. Solids Struct. 38 (2) (2001) 183–201.
[63] L.Z. Sun, J.W. Ju, Effective elastoplastic behavior of metal matrix composites containing randomly located aligned spheroidal inhomogeneities. Part II: applications, Int. J. Solids Struct. 38 (2) (2001) 203–225.
[64] L.Z. Sun, J.W. Ju, Elastoplastic modeling of metal matrix composites containing randomly located and oriented spheroidal particles, J. Appl. Mech-T ASME 71 (2004) 774–785.
[65] P. Sheng, Effective-medium theory of sedimentary rocks, Phys. Rev. B 41 (1990) 4507–4512.
[66] H.H. Zhu, Q. Chen, J.W. Ju, Z.G. Yan, F. Guo, Y.Q. Wang, Z.W. Jiang, S. Zhou, B. Wu, Maximum entropy based stochastic micromechanical model for two-phase composite considering the inter-particle interaction effect, Acta Mech. 226 (9) (2015) 3069–3084.
[67] H.H. Zhu, Q. Chen, Z.G. Yan, J.W. Ju, S. Zhou, Micromechanical model for saturated concrete repaired by electrochemical deposition method, Mater. Struct. 47 (2014) 1067–1082.
[68] Z.G. Yan, Q. Chen, H.H. Zhu, J.W. Ju, S. Zhou, Z.W. Jiang, A multiphase micromechanical model for unsaturated concrete repaired by electrochemical deposition method, Int. J. Solids Struct. 50 (24) (2013) 3875–3885.
[69] Q. Chen, H.H. Zhu, J.W. Ju, F. Guo, L.B. Wang, Z.G. Yan, T. Deng, S. Zhou, A stochastic micromechanical model for multiphase composite containing spherical inhomogeneities, Acta Mech. 226 (6) (2015) 1861–1880.
[70] Q. Chen, H.H. Zhu, Z.G. Yan, T. Deng, S. Zhou, Micro-scale description of the saturated concrete repaired by electrochemical deposition method based on Mori–Tanaka method, J. Build. Struct. 36 (1) (2015) 98–103.
[71] Q. Chen, H.H. Zhu, Z.G. Yan, J.W. Ju, T Deng, S. Zhou, Micro-scale description of the saturated concrete repaired by electrochemical deposition method based on self-consistent method, Chin. J. Theor. Appl. Mech. 47 (2) (2015) 367–371.
[72] Q. Chen, Z.W. Jiang, Z.H. Yang, H.H. Zhu, J.W. Ju, Z.G. Yan, Y.Q. Wang, Differential-scheme based micromechanical framework for saturated concrete repaired by the electrochemical deposition method, Mater. Struct. (2016), http://dx.doi.org/10.1617/s11527-016-0853-1.
[73] M. MousaviNezhad, H.H. Zhu, J.W. Ju, Q. Chen, A simplified multiscale damage model for the transversely isotropic shale rocks under tensile loading, Int. J. Damage Mech (2016), http://dx.doi.org/10.1177/1056789516639531.
[74] R.M. Christensen, K.H. Lo, Solutions for effective shear properties in three phase sphere and cylinder models, J. Mech. Phys. Solids 27 (1979) 315–330.
[75] J.C. Halpin, J.L. Kardos, The Halpin–Tsai equations: a review, Polym. Eng. Sci. 16 (1976) 344–352.
[76] P.A. Wall, Comparison of homogenization, Hashin–Shtrikman bounds and the Halpin–Tsai equations, Appl. Math. 42 (4) (1997) 245–257.
[77] G.R. Williamson, The effect of steel fibers on the compressive strength of concrete, International Symposium on Fiber Reinforced Concrete, SP 44-11, Am ConcrInst (1974) 195–207.
[78] A.F. Stock, D.J. Hannant, R.I.T. Williams, The effect of aggregate concentration upon the strength and modulus of elasticity of concrete, Mag. Concr. Res. 31 (109) (1979) 225–234.
[79] C.J. Jiao, Z.F. Zhan, C.Y. Peng, W.H. Zhang, Experimental study of hybrid fiber reinforced concrete under compression, J. Guangzhou Univ. 6 (4) (2007) 70–73.
[80] E.T. Dawood, M. Ramli, Mechanical properties of high strength flowing concrete with hybrid fibers, Constr. Build. Mater. 28 (2012) 193–200.